Journal of Cerebral Blood Flow & Metabolism (2011) 31, 560–571

www.jcbfm.com

Similarities and differences in arterial responses to hypercapnia and visual stimulation

Yi-Ching Lynn Ho[1,2], Esben Thade Petersen[1,2,3], Ivan Zimine[1,4] and Xavier Golay[1,5]

[1]*Department of Neuroradiology, National Neuroscience Institute, Singapore, Singapore;* [2]*Center for Functionally Integrative Neuroscience, Aarhus University, Aarhus, Denmark;* [3]*Clinical Imaging Research Centre, Singapore, Singapore;* [4]*Clinical Science, Philips Healthcare, Tokyo, Japan;* [5]*Department of Brain Repair and Rehabilitation, UCL Institute of Neurology, Queen Square, London, UK*

Despite the different origins of cerebrovascular activity induced by neurogenic and nonneurogenic conditions, a standard assumption in functional studies is that the consequence on the vascular system will be mechanically similar. Using a recently developed arterial spin labeling method, we examined arterial blood volume, arterial-microvascular transit time, and cerebral blood flow (CBF) in the gray matter and in areas with large arterial vessels under hypercapnia, visual stimulation, and a combination of the two. Spatial heterogeneity in arterial reactivity was observed between conditions. During hypercapnia, large arterial volume changes contributed to CBF increase and further downstream, there were reductions in the gray matter transit time. These changes were not significant during visual stimulation, and during the combined condition they were moderated. These findings suggest distinct vascular mechanisms for large and small arterial segments that may be condition specific. However, the power relationships between gray matter arterial blood volume and CBF in hypercapnia ($\alpha = 0.69 \pm 0.24$) and visual stimulation ($\alpha = 0.68 \pm 0.20$) were similar. Assuming consistent capillary and venous volume responses across these conditions, these results offer support for a consistent total CBV–flow relationship typically assumed in blood oxygen-level dependent calibration techniques.
Journal of Cerebral Blood Flow & Metabolism (2011) **31,** 560–571; doi:10.1038/jcbfm.2010.126; published online 11 August 2010

Keywords: cerebral blood flow; cerebral hemodynamics; experimental; functional MRI; neurophysiology

Introduction

Cerebral blood flow (CBF) is constantly adjusting to suit the specific needs of the brain. It is well known that brain stimulation through cognitive tasks or sensory presentation results in CBF increase, which could be driven by neurotransmitter release (Attwell and Iadecola, 2002) and the demand for oxygen on a local level (Buxton and Frank, 1997). Cerebral blood flow changes can also be caused by simply manipulating the vascular system using pharmacological substances or respiratory gases. For example, CO_2 inhalation causes CBF to increase through the increased perivascular presence of H+ (Kuschinsky *et al*, 1972) and is assumed not to significantly modulate oxidative metabolism (Kety and Schmidt, 1948). Therefore, hypercapnia is used as a standard method to calibrate the blood oxygen-level dependent (BOLD) signal (Davis *et al*, 1998).

Nonetheless, it is clear that CBF, the delivery rate of arterial blood to the tissue capillary bed, is a complex phenomenon. There are large variations in CBF and other vascular responses between and within subjects that have been observed in several studies (Hutchinson *et al*, 2006; Leontiev and Buxton, 2007; Ito *et al*, 2008), and which may not simply be attributed to measurement errors (Leontiev and Buxton, 2007; Piechnik *et al*, 2008). For example, variability in oxidative demand (Leontiev and Buxton, 2007) and vascular tone (Ito *et al*, 2008) may partly explain CBF variability both at baseline and during functional activity.

Furthermore, it seems that the type of physiologic or functional challenge presented may influence the nature of vascular reactivity that governs CBF changes. Britz *et al* (2007) showed that subarachnoid hemorrhage in a rat model attenuated arteriolar dilation induced by somatosensory stimulation, even though somatosensory-evoked potentials were unaffected. At the same time, hypercapnia-induced

Correspondence: Dr Y-CL Ho, Department of Neuroradiology, Center for Functionally Integrative Neuroscience, Aarhus University, 5th floor, Building 10G, 44 Norrebrogade, Aarhus C 8000, Denmark. E-mail: yiching.lynn.ho@gmail.com
This study was supported by a grant from the National Medical Research Council (NMRC/0855/2004). Y-CL Ho was supported by the Singapore Millennium Foundation.
Received 17 February 2010; revised 8 June 2010; accepted 5 July 2010; published online 11 August 2010

arteriolar dilation was not impaired. These intriguing results in rats draw attention to the different mechanisms involved in CBF regulation and the implications for function and recovery in altered states like disease. There is currently scant literature especially on healthy humans that compare the vascular responses elicited during different functional challenges, especially between neurogenic and nonneurogenic conditions.

Cerebral blood flow and various aspects of vascular reactivity can be studied noninvasively using a relatively new magnetic resonance imaging technique based on arterial spin labeling (ASL)—QUASAR (quantitative STAR (signal targeting by alternating radiofrequency) labeling of arterial regions) (Petersen *et al*, 2006). By comparing the ASL signal acquired with and without large arterial inflow components, this technique allows the extraction of several vascular parameters: CBF, the blood volume of large arterial vessels (aBV_{LV}), the arterial blood volume within the gray matter (aBV_{GM}), and the arrival time of blood at the respective compartments within the voxel containing large vessel arterial blood ($\tau_{a,LV}$), gray matter arterial blood ($\tau_{a,GM}$), and the microvascular (τ_m) portion within the tissue. Functional changes in CBF and the microvascular arrival time estimated with this technique have been previously assessed to be comparable with those estimated by a standard three-parameter fit of the general kinetic model (Ho *et al*, 2010). On the basis of these vascular parameters, the primary aim of this study was to investigate whether CBF increases in both visual stimulation and hypercapnia would be governed by different vascular responses.

As a secondary aim, we also used three vascular crushing gradients with the velocity-encoding level ('Venc') at 3, 6, and 9 cm/s to investigate whether targeting different 'depths' of the arterial tree would affect the estimation and statistical significance of the vascular parameters. Bipolar crusher gradients have been used in ASL to dephase water spins flowing past a certain velocity to estimate tissue perfusion more accurately (Ye *et al*, 1997). In the model-free QUASAR technique, bipolar crusher gradients are also used to delineate the macrovascular (arterial) and microvascular compartments. Given that capillary blood velocities are ~ 0.1 cm/s or lower, as found in animal studies (Villringer *et al*, 1994; Kleinfeld *et al*, 1998; Hutchinson *et al*, 2006), the rationale is to use as low a velocity-encoding level as possible without losing too much detection power, especially with the typical ASL perfusion-weighted signal change already being very small. At Venc = 3 cm/s, one is likely to be probing arterioles and perhaps small arteries in addition to capillaries as part of the microvascular compartment, because arterioles and small pial arteries of diameter $< 200\,\mu$m appear to have flow velocities that range from 1 to 6 cm/s (Kobari *et al*, 1984; Gilmore *et al*, 2005; Kisilevsky *et al*, 2008). Decreasing the bipolar crushing gradients, or in other words, using higher levels of velocity encoding, such as 6 cm/s ($b = 0.32$ seconds/mm^2) and 9 cm/s ($b = 0.14$ seconds/mm^2) would still exclude significant arterial signal, given that the large conductive arteries in the human brain are known to have flow velocities of 30 cm/s and beyond, as measured in the posterior, middle, and anterior cerebral arteries. It is unclear whether the level of vascular crushing has an effect on the observed interactions of the relative relationships of the hemodynamic parameters and we sought to investigate this.

Materials and methods

Functional Magnetic Resonance Imaging Experiments

All experiments were performed on a clinical 3.0-T scanner (Philips Healthcare, Best, The Netherlands) using a standard setup of body coil transmission and an eight-channel SENSE head coil for reception.

Perfusion-weighted scans were performed using the ASL QUASAR sequence (Petersen *et al*, 2006), which combines a modified STAR sequence with a GRE-EPI (gradient recalled echo-echo planar imaging), Look–Locker readout strategy (Gowland and Mansfield, 1993) for sampling at multiple inversion time points and a QUIPSS II (quantitative imaging of perfusion using a single subtraction, 2nd version) bolus saturation scheme for clear definition of the arterial blood bolus (Wong *et al*, 1998). The parameters were: repetition time/echo time = 3,000/21 milliseconds, flip angle = 35°, ΔTI = 200 milliseconds, inversion time points = 14, τ_b = 640 milliseconds, SENSE factor = 2.5, labeling slab = 150 mm, inversion gap = 30 mm, field of view = 224×224 mm^2, matrix = 64×64, slices = 3, slice thickness = 5 mm. Each QUASAR scan was performed four times while varying the velocity encoding or bipolar crusher gradients (Venc = 3, 6, 9 cm/s or no crushers in the foot–head direction). For each scan, there were 123 pairs of control and labeled images and each scan time = 12 minutes 18 seconds. Slices were aligned to the calcarine sulcus, with the help of a T_1-weighted sagittal scan (repetition time = 3,800 milliseconds, echo time = 15 milliseconds, flip angle = 90°, matrix = 512×512).

Eight healthy volunteers (two men, six women; age range 26–44 years) gave informed, written consent before participation. The protocol was approved by the Institutional Review Board. One subject had the last scan (out of four) aborted because of time constraints.

The functional paradigm consisted of a gray-scale, 8 Hz radial checkerboard pattern with 2 levels of visual contrast (25% and 100%) that alternated with a baseline condition of an iso-luminance gray (50%) background. Presentation of the visual stimuli was carried out using the Eloquence System (Invivo, Orlando, FL, USA) that was mounted onto the head coil.

Each run consisted of two main segments: The first segment consisted of 5 baseline blocks (15 EPI volumes each) that alternated with 4 visual blocks (10 EPI volumes each) with the subject breathing a normal air mixture. The second segment consisted of the same visual paradigm, but with the subject breathing a hypercapnic gas mixture of

21% O_2 and a proportion of CO_2 that aimed to increase each subject's end-tidal pCO_2 levels by approximately a third of the baseline. The balance of the gas mixture comprised N_2. In between the first and second segments, there was a rest period of 1 minute 30 seconds for introduction of the gas mixture and stabilization of the physiologic parameters. For each of the four QUASAR scans that varied the velocity encoding, the same experimental design was used.

End-tidal pCO_2, heart rate, respiratory rate, and oxygen saturation for each subject were monitored continuously using a magnetic resonance-compatible patient monitoring system with a pulse oximeter (Invivo). Hudson RCI nonrebreathing masks (Hudson Respiratory Care, Durham, NC, USA) were fitted for each subject.

Data Processing

Postprocessing was carried out on a Windows PC using in-house programs written in IDL 6.1 (ITT Visual Information Solutions, Boulder, CO, USA). The procedures are similar to the methods detailed in the study by Ho *et al* (2010).

Data from one subject had to be discarded because of motion artifacts. For all other data, linear interpolation of both control and labeled data was performed before any subtraction to match the BOLD effects for each time point. Subsequent pairwise subtraction of the interpolated labeled data from the interpolated control data resulted in perfusion-weighted images ($\Delta M(t)$). The first 3 volumes (9 seconds) of each visual block and the first 5 volumes (15 seconds) of each baseline block were excluded from the analyses to ensure steady-state measurements. Wilcoxon's rank-sum tests ($P<0.001$, uncorrected for multiple comparisons) were performed voxel by voxel, with a cluster threshold of three voxels to determine the regions of interest (ROIs). The intersection of significantly activated voxels in all scans and conditions were then taken as the final ROI for each subject.

Within each subject and experimental condition (the 100% and 25% visual contrast conditions were averaged together for simplicity), three curves were derived: (1) the tissue curve ($\Delta M_{cr}(t)$ of the crushed data), (2) the arterial input function for the deconvolution, based on voxels with large arterial contribution (AIF_{LV}), and (3) the 'gray matter' AIF (AIF_{GM}). A subtraction of $\Delta M_{cr}(t)$ from $\Delta M_{ncr}(t)$ would provide the AIF for each voxel. The area under the AIF represents the arterial blood volume and can be obtained by integration of the curve. AIF_{LV} was averaged from the two voxels with the consistently largest arterial blood volumes within the significantly activated voxels in all conditions. The same two AIF sampling voxels were used in all conditions for each subject. AIF_{GM} was based on a subtraction of $\Delta M_{cr}(t)$ from $\Delta M_{ncr}(t)$ averaged from the ROI, but excluding the two voxels for AIF sampling. (AIF_{GM} was not used in the deconvolution process to estimate CBF, but it provides additional information about the small arterial compartment in the ROI, which can be said to contain largely the gray matter.) The areas under AIF_{LV} and AIF_{GM} provided estimates of the arterial blood volumes of large vessels (aBV_{LV}) and gray matter (aBV_{GM}). These parameters were corrected by the factors outlined in Equations 2 and 3 in the study by Ho *et al* (2010). The large vessel arterial arrival time ($\tau_{a,LV}$), the gray matter arterial arrival time ($\tau_{a,GM}$), and the microvascular arrival time (τ_m) were estimated from the rising edges of AIF_{LV} for deconvolution, AIF_{GM}, and tissue curve, respectively. From these, we derived the arterial-microvascular transit time for large vessel ($TT_{am,LV}$) and gray matter areas ($TT_{am,GM}$) by calculating ($\tau_m-\tau_{a,LV}$) and ($\tau_m-\tau_{a,GM}$), respectively. Figure 1 is a schematic diagram of the arterial and microvascular compartments and how they relate to the three curves and various parameters.

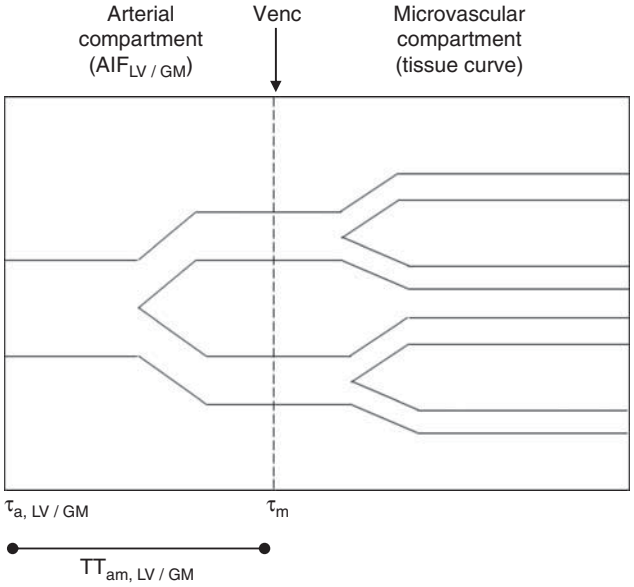

Figure 1 Schematic diagram of the arterial and microvascular compartments and how they relate to the arterial input function (AIF) and the tissue curve. Both τ_a and τ_m are the respective arrival times of the bolus to the arterial and microvascular compartments in a voxel, whereas TT_{am}, the arterial-microvascular transit time, is the difference of the two arrival times. The boundary between the arterial and microvascular compartment is set by the velocity-encoding level (Venc). We distinguish between two spatial areas containing arterial blood: 'large vessel' and 'gray matter,' and their respective parameters are labeled with the appropriate subscripts.

Using the method described in the study by Petersen *et al* (2006), CBF for each condition was quantified by truncated singular value decomposition of the general kinetic model (Buxton *et al*, 1998):

$$\Delta M(t) = 2 \cdot M_{a,0} \cdot f \cdot \int_0^t C_a(t) \cdot r(t-\tau) \cdot m(t-\tau) d\tau,$$

where $M_{a,0}$ is the equilibrium magnetization for arterial blood, f the flow, $C(t)$ the AIF, $r(t-\tau)$ the residue function describing the clearance of spin from the tissue, and $m(t-\tau)$ the longitudinal magnetization relaxation. $M_{a,0}$ was estimated for each subject by fitting the saturation recovery curve of the gray matter, taking into account slice profile effects and assuming the gray matter, brain–blood partition

coefficient for water, $\lambda = 0.98$ (Herscovitch and Raichle, 1985).

Statistical Analysis

Statistical analyses were performed using R version 2.7.2 (The R Foundation for Statistical Computing, Vienna, Austria) and SPSS version 13 (SPSS, Chicago, IL, USA). All parameters were checked for normality before the parametric analyses. The statistical significance threshold was set at 0.05.

Given the multiple within-subject variables, linear mixed models using the restricted maximum likelihood estimation were used to assess the effect of the fixed factors of velocity-encoding level, visual stimulation, and hypercapnia on each vascular parameter (CBF, aBV_{LV}, $\tau_{a,LV}$, τ_m, aBV_{GM}, $\tau_{a,GM}$), with the random factor being the subject. The fixed factor of the velocity-encoding level was analyzed, followed by the effects of visual stimulation and hypercapnia on each vascular parameter, which were analyzed at each separate level of velocity encoding. This was done to ensure that the velocity-encoding level did not influence relationships of the vascular parameters during visual stimulation and hypercapnia in complex ways. Interactions between conditions of visual stimulation and hypercapnia were also assessed.

Fractional changes for the experimental conditions of hypercapnia alone, visual stimulation alone, and combined hypercapnia and visual stimulation were calculated from pure baseline (normocapnia and visual baseline). The results were averaged across all three velocity-encoding levels, because the linear mixed model analysis would find no significant interaction between the effects of velocity-encoding level, hypercapnia, and visual stimulation. One-sample *t*-tests were used to assess the significance of the fractional changes from baseline. Assuming the relationship between changes in CBF and aBV_{LV}, as well as changes in CBF and aBV_{GM}, are best described by power law relationships, α, the exponent was calculated for each data set as $\ln(1+\Delta aBV_{LV\ or\ GM}/aBV_{LV\ or\ GM})/\ln(1+\Delta CBF/CBF)$. Paired *t*-tests and Wilcoxon's rank-sum tests were used to compare α-values in the different conditions.

Results

End-tidal pCO_2 across subjects in the hypercapnic condition was 54 ± 3 mm Hg (mean and s.d.), an increase of $35\% \pm 7.5\%$. Subject wellbeing was monitored with the physiologic parameters of oxygen saturation, heart rate, and respiratory rate. Oxygen saturation across subjects was maintained at 0.98 ± 0.01 throughout the conditions. Heart rate did not change significantly with hypercapnia (a difference of 2.4 ± 4.5 beats per minute) and neither did the respiratory rate (a difference of -1.1 ± 1.5 breaths per minute), as shown with paired *t*-tests.

Figure 2A shows the AIFs and tissue curves in each condition from a typical subject. The tissue curves during visual stimulation were higher in magnitude and slightly faster in arrival as compared with no stimulation. The AIFs tended to be larger and started earlier during hypercapnia (and particularly with visual stimulation in this subject). With higher velocity encoding (smaller bipolar gradients), AIFs became diminished, whereas tissue curves became faster and enlarged. For the same subject, the ROI (in red) and the sites of AIF sampling (in orange) are overlaid onto a perfusion-weighted image and shown in Figure 2B.

Figure 3 illustrates the main effect of velocity encoding on the estimation of various vascular parameters, which have been averaged across the conditions of visual stimulation and hypercapnia. The estimation of CBF was not significantly affected by the different velocity-encoding levels. However, aBV_{LV} and aBV_{GM} estimations were significantly smaller at Venc = 3 cm/s compared with the other two levels. Similarly, $\tau_{a,LV}$ and $\tau_{a,GM}$ estimations were significantly shorter at Venc = 3 cm/s versus the other two levels. Estimation of τ_m significantly diminished with each step-up of velocity encoding. Separate analyses for each of the three levels of velocity encoding assessing the effects of visual stimulation and hypercapnia on each vascular parameter showed consistency in the pattern of responses found at each velocity-encoding level. There were no significant interactions between velocity-encoding level and the effects of visual stimulation and hypercapnia.

Table 1 reports the mean values with confidence intervals for each vascular parameter during pure baseline (normocapnia/visual baseline), during hypercapnia alone (visual baseline), during visual stimulation alone (normocapnia), and during combined hypercapnia and visual stimulation. The fractional changes (mean ± s.e.m. (%)) from pure baseline for each vascular parameter in each condition are also reported. The values were averaged across all velocity-encoding levels, given that the patterns of change in both functional challenges were consistent across the velocity-encoding levels. During baseline, aBV_{GM} was significantly smaller than aBV_{LV}, whereas $\tau_{a,GM}$ was significantly later than $\tau_{a,LV}$, showing that the gray matter arterial compartment within the ROI reflects smaller arterial vessels downstream of the large arterial vessels within the AIF sampling sites.

The apparent difference in the trends of the fractional changes for the conditions of hypercapnia alone, visual stimulation alone, and hypercapnia with visual stimulation combined are further illustrated in Figure 4. (The collective responses of the arrival times, $\tau_{a,LV}$, $\tau_{a,GM}$, and τ_m, can be realized in the transit times, $TT_{am,LV}$ and $TT_{am,GM}$, and thus we will subsequently concentrate on the transit times when considering timing responses). During hypercapnia, the increase in aBV_{LV} was approximately half of the CBF increase. In the other two conditions of visual stimulation and the combined effect of hypercapnia and visual stimulation, CBF increases were accompanied by much smaller aBV_{LV} increases: the aBV_{LV} increase with visual stimulation alone did not reach

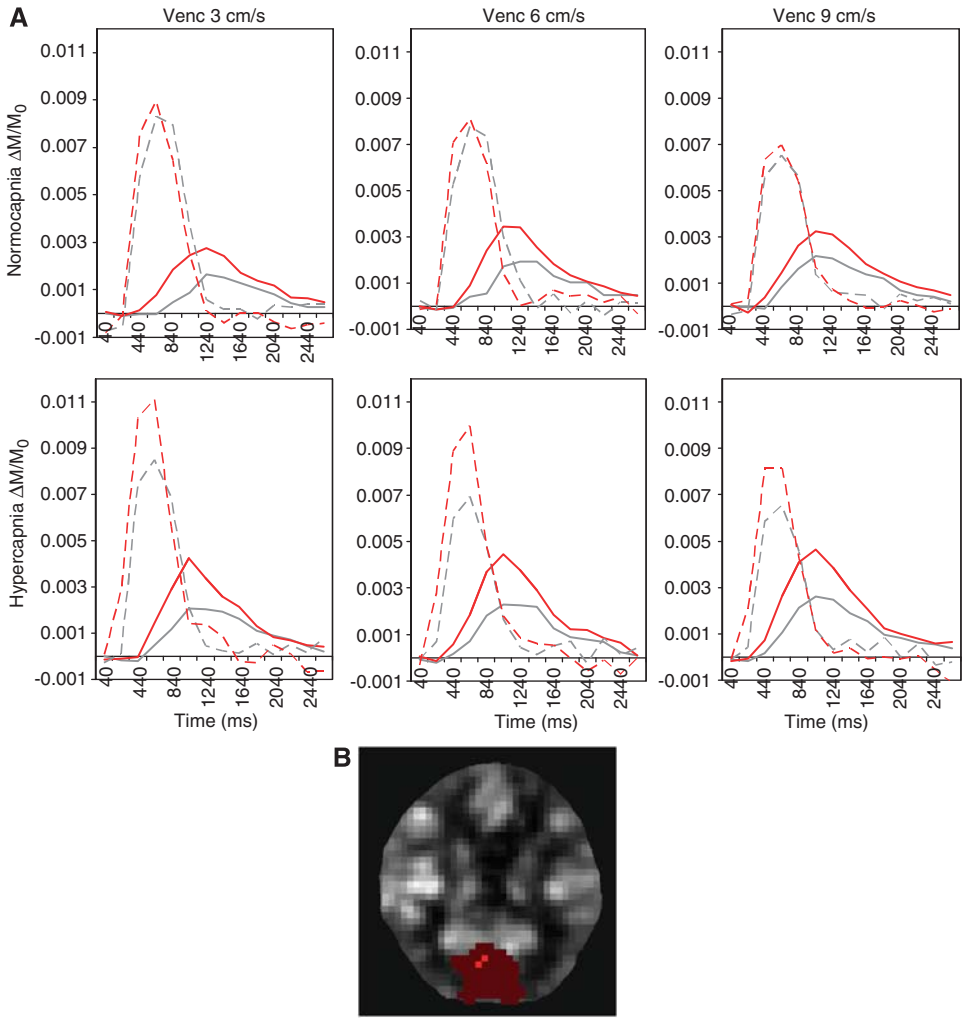

Figure 2 Example of perfusion-weighted data from one typical subject: (**A**) Fractional AIF_{LV} (broken lines) and tissue curves (solid lines) within each condition. ΔTI was 200 milliseconds. The gray and red lines represent rest and stimulation, respectively, in the visual condition. The top row shows normocapnic data, whereas the bottom row shows hypercapnic data. The columns show the results for the velocity-encoding levels of 3, 6, and 9 cm/s. (**B**) The ROI (red) with the sites of AIF_{LV} sampling (orange) overlaid onto a perfusion-weighted ΔM baseline image of the same subject. AIF, arterial input function; ROI, region of interest.

statistical significance, whereas the aBV_{LV} increase in the combined condition was ~15% that of the CBF increase. There were significant reductions in $TT_{am,LV}$ in each condition that corresponded inversely to the strength of the respective CBF increases. Separate from large arterial reactivity, aBV_{LV} in the gray matter (aBV_{GM}) appeared to increase in consistent proportion to CBF increases across the experimental conditions (approximate ratio of half, although the aBV_{GM} increase in hypercapnia alone did not reach statistical significance). There were significant reductions in $TT_{am,GM}$ for the hypercapnia and combined conditions.

Figure 5 illustrates the differences in α-values (mean ± s.e.m.) calculated for the change in blood volume compared with the change in flow in each experimental condition. A couple of outliers that exceeded two s.d. were excluded from the analyses in each condition. Including them in the analyses did not make a difference to the pattern of results. The α-values for the relationships between aBV_{GM} and CBF in all three conditions were relatively high, ranging from 0.55 ± 0.12 to 0.69 ± 0.24, and they were not significantly different from each other. A higher α-value indicates a larger dependence of flow on the volume change. The large vessel aBV_{LV}–CBF relationship is clearly different between hypercapnia and visual stimulation—during hypercapnia, the α-value for the aBV_{LV}–CBF relationship is a high 0.68 ± 0.15 (similar to that of the aBV_{GM}–CBF relationship). Conversely, with visual stimulation, the α-value for the aBV_{LV}–CBF relationship was not significantly different from zero, indicating an insignificant contribution of aBV_{LV} to CBF changes with visual stimulation. The combined condition yielded a mean α-value of 0.18 ± 0.05, showing a relatively low but significant dependence of flow on aBV_{LV}. Paired *t*-tests and Wilcoxon's rank-sum tests showed significant differences between the α-values in hypercapnia

compared with visual stimulation, and also between hypercapnia and the combined condition.

Figure 6 shows the scatterplots of (panel A) $\Delta aBV_{LV}/aBV_{LV}$ with $\Delta CBF/CBF$, (panel B) $\Delta aBV_{GM}/aBV_{GM}$ with $\Delta CBF/CBF$, (panel C) $\Delta aBV_{LV}/aBV_{LV}$ with $\Delta TT_{am,LV}/TT_{am,LV}$, and (panel D) $\Delta aBV_{GM}/aBV_{GM}$ with $\Delta TT_{am,GM}/TT_{am,GM}$. There were highly significant, linear relationships between $\Delta aBV_{LV}/aBV_{LV}$ with $\Delta TT_{am,LV}/TT_{am,LV}$ in both hypercapnia (slope = 0.53 ± 0.16, $P = 0.003$) and visual stimulation (slope = 0.61 ± 0.13, $P < 0.001$). The relationship did not reach statistical significance in the combined condition. The linear relationships between $\Delta aBV_{GM}/aBV_{GM}$ with $\Delta TT_{am,GM}/TT_{am,GM}$ in each condition were not statistically significant.

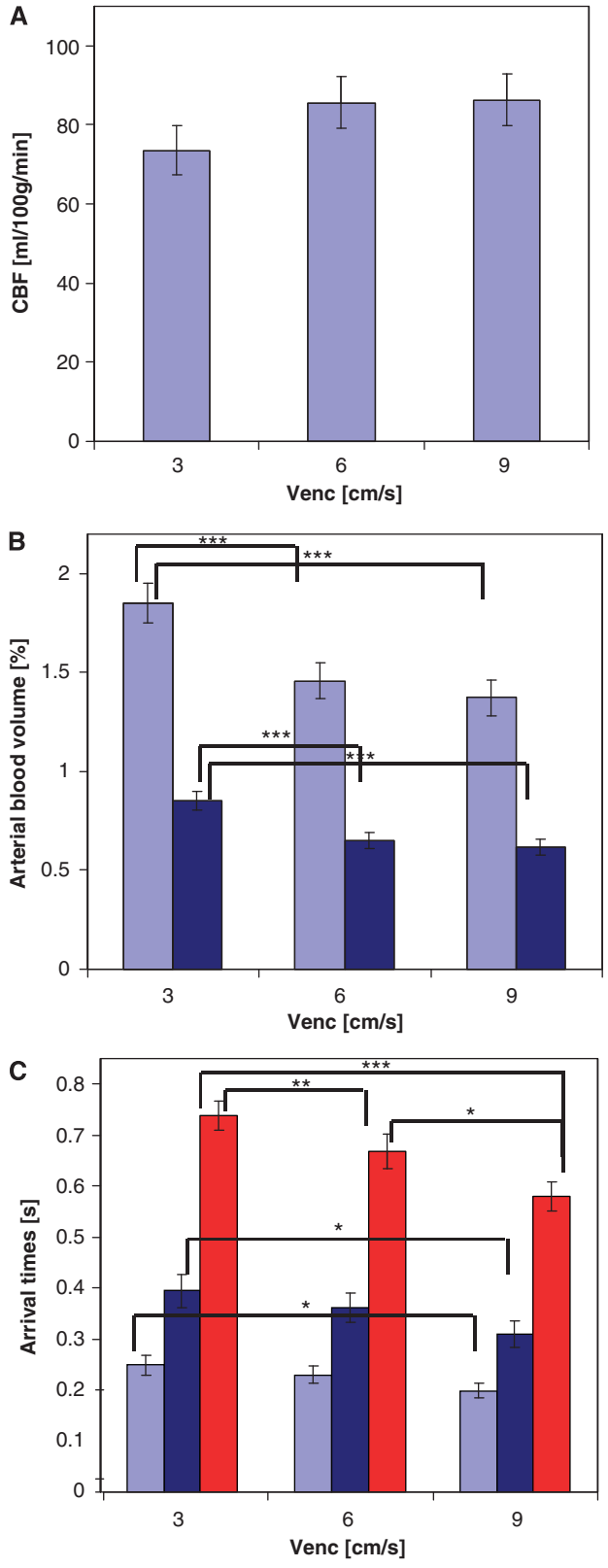

Discussion

Effect of Velocity-Encoding Levels on Parameter Estimation

aBV_{LV}, aBV_{GM}, and τ_m estimations were the most highly affected by the different velocity-encoding levels, because these two parameters depend most directly on the macrovascular–microvascular boundary, which is set between the small reactive arteries to the arterioles. Using higher levels of velocity encoding (or smaller bipolar crushing gradients) shifts this artificial boundary toward the arterial side, i.e., diminishing the arterial compartment and therefore also the aBV_{LV} and aBV_{GM} estimation, which is in line with the results obtained from the study by Brookes *et al* (2007). Reducing vascular crushing also enlarges the 'microvascular' compartment and hence τ_m appeared shorter. At the three levels of velocity encoding that we used, we found that CBF estimation through the model-free method was not significantly altered, and that there was consistency across these levels in response of vascular parameters to hypercapnia and visual stimulation. This is reassuring for functional studies of perfusion using this range of velocity-encoding levels.

It should be pointed out that possible artifactual changes in compartments may occur because blood velocities may change with functional challenges and the level of velocity encoding is typically constant between baseline and functional challenge. Velocity increases of up to 45% have been found with functional challenges in various arterial vessels: in human retinal arterioles during hypercapnia (Kisilevsky *et al*, 2008), in the small pial arteries of

Figure 3 The effect of velocity encoding on vascular parameter estimation. (**A**) CBF, (**B**) aBV_{LV} (light blue), aBV_{GM} (dark blue), and (**C**) $\tau_{a,LV}$ (light blue), $\tau_{a,GM}$ (dark blue) and τ_m (red). The values have been averaged over the visual stimulation and hypercapnia conditions. The bars represent mean values ± s.e.m. Significant differences are marked by asterisks (***$P \leq 0.001$, **$P \leq 0.01$, *$P \leq 0.05$). aBV_{GM}, arterial blood volume within the gray matter; aBV_{LV}, blood volume of large arterial vessel; CBF, cerebral blood flow; $\tau_{a,LV}$, large vessel arterial blood.

Table 1 Mean values with confidence intervals in brackets for each of the vascular parameters in pure baseline (normocapnia/visual baseline), in hypercapnia alone (visual baseline), in visual stimulation alone (normocapnia), and in combined hypercapnia and visual stimulation

	CBF (ml/100 g/min)	*aBV_{LV} (%)*	*$\tau_{a,LV}$ (seconds)*	*τ_m (seconds)*	*$TT_{am,LV}$ (seconds) i.e., ($\tau_m - \tau_{a,LV}$)*	*aBV_{GM} (%)*	*$\tau_{a,GM}$ (seconds)*	*$TT_{am,GM}$ (seconds) i.e., ($\tau_m - \tau_{a,GM}$)*
Pure baseline	57 (48, 65)	1.47 (1.21, 1.73)	0.27 (0.23, 0.31)	0.77 (0.69, 0.85)	0.50 (0.45, 0.55)	0.60 (0.50, 0.70)	0.40 (0.32, 0.48)	0.37 (0.32, 0.42)
Hypercapnia alone	68 (57, 78) 21% ± 5%	1.59 (1.33, 1.85) 11% ± 4%	0.22 (0.18, 0.26) −18% ± 2%	0.67 (0.59, 0.75) −13% ± 2%	0.45 (0.40, 0.50) −9% ± 3%	0.66 (0.53, 0.80) 11% ± 6%	0.37 (0.30, 0.45) −5% ± 5%	0.30 (0.25, 0.34) −17% ± 7%
Visual stimulation alone	86 (76, 96) 64% ± 12%	1.55 (1.34, 1.77) 10% ± 5%	0.23 (0.18, 0.28) −16% ± 4%	0.64 (0.58, 0.71) −16% ± 2%	0.41 (0.38, 0.45) −14% ± 4%	0.73 (0.64, 0.82) 28% ± 8%	0.34 (0.27, 0.41) −13% ± 3%	0.30 (0.26, 0.34) −13% ± 8%
Combined hypercapnia and visual stimulation	116 (100, 132) 111% ± 8%	1.67 (1.39, 1.94) 16% ± 4%	0.19 (0.16, 0.22) −30% ± 2%	0.58 (0.52, 0.65) −24% ± 2%	0.40 (0.35, 0.44) −20% ± 3%	0.85 (0.75, 0.95) 53% ± 13%	0.31 (0.25, 0.37) −22% ± 4%	0.27 (0.25, 0.30) −20% ± 7%

aBV_{GM}, arterial blood volume within the gray matter; aBV_{LV}, blood volume of large arterial vessel; CBF, cerebral blood flow; $\tau_{a,GM}$, arrival time of blood at the respective compartments within the voxel containing gray matter arterial blood; $\tau_{a,LV}$, arrival time of blood at the respective compartments within the voxel containing large vessel arterial blood; τ_m; arrival time of blood at the respective compartments within the voxel containing the microvascular portion within the tissue; $TT_{am,GM}$, arterial-microvascular transit time for the gray matter; $TT_{am,LV}$, arterial-microvascular transit time for large vessel.
The values were averaged across all velocity-encoding levels. The percentage changes from pure baseline for each condition are also reported (mean ± s.e.m.).

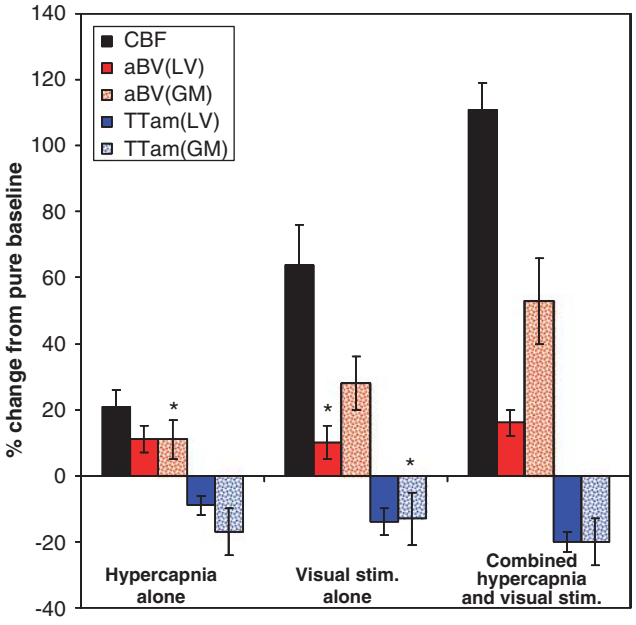

Figure 4 The trends of the fractional changes for the conditions of hypercapnia alone, visual stimulation alone, and hypercapnia with visual stimulation combined. Asterisks (*) mark the changes that were *not* statistically significant. aBV_{GM} and TT_{am} show changes proportional to CBF changes across the three conditions. aBV_{GM}, arterial blood volume within the gray matter; CBF, cerebral blood flow; TT_{am}, arterial-microvascular transit time.

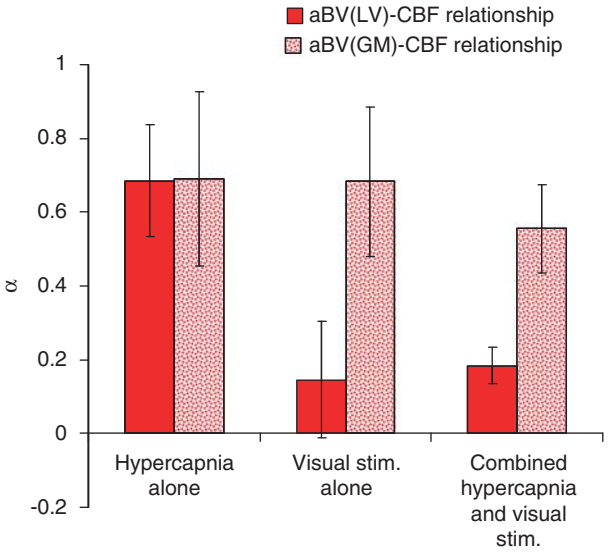

Figure 5 Differences in the α-values (mean ± s.e.m.), calculated for the change in blood volume compared with the change in flow in each experimental condition. The α-value for the aBV_{LV}–CBF relationship in visual stimulation was not significantly different from zero. aBV_{LV}, blood volume of large arterial vessel; CBF, cerebral blood flow.

cats during hypercapnia (Kobari *et al*, 1984), in the human posterior cerebral artery during visual stimulation (Panczel *et al*, 1999), and during hypercapnia in the middle cerebral artery (Kisilevsky *et al*, 2008).

Given that our 'microvascular' compartment probably includes arterioles and even small arteries, a velocity increase during a functional challenge could thus result in a baseline 'microvascular' segment becoming reclassified as part of the 'arterial' segment during the functional challenge, if there is blood that now travels faster than the velocity-encoding

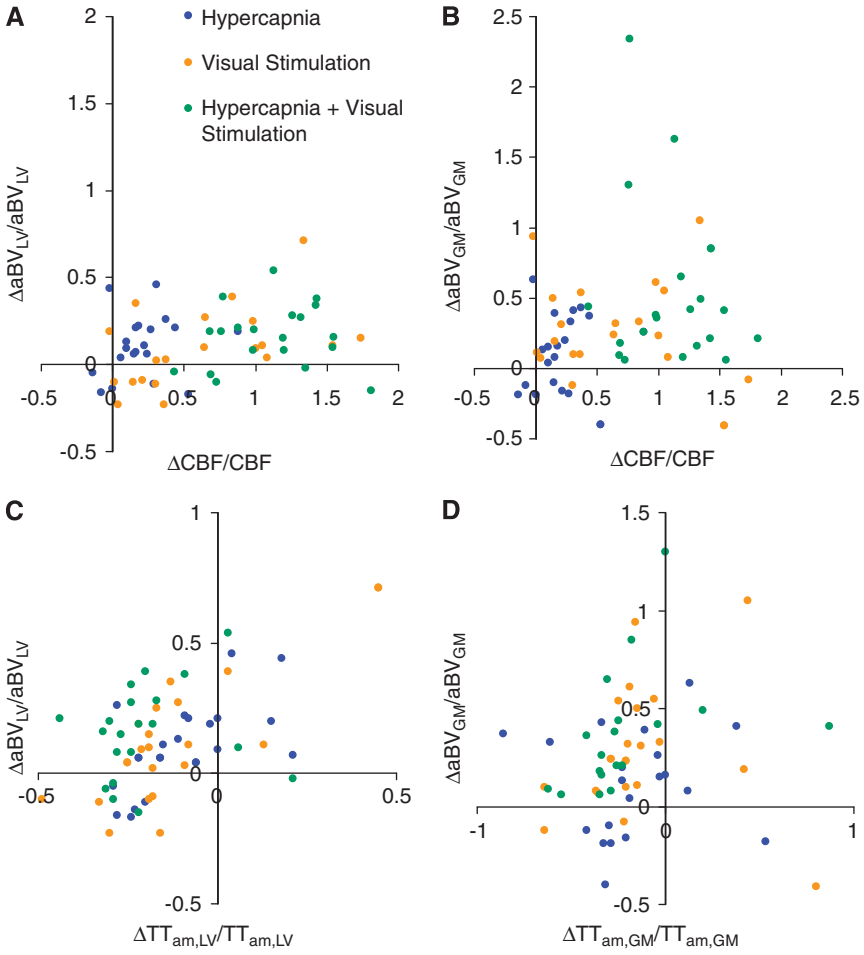

Figure 6 Scatterplots of the fractional changes in arterial blood volumes with CBF and transit times in the three experimental conditions. (**A**) $\Delta aBV_{LV}/aBV_{LV}$ with $\Delta CBF/CBF$, (**B**) $\Delta aBV_{GM}/aBV_{GM}$ with $\Delta CBF/CBF$, (**C**) $\Delta aBV_{LV}/aBV_{LV}$ with $\Delta TT_{am,LV}/TT_{am,LV}$, and (**D**) $\Delta aBV_{GM}/aBV_{GM}$ with $\Delta TT_{am,GM}/TT_{am,GM}$. aBV_{GM}, arterial blood volume within the gray matter; aBV_{LV}, blood volume of large arterial vessel; CBF, cerebral blood flow; $TT_{am,GM}$, arterial-microvascular transit time for the gray matter; $TT_{am,LV}$, arterial-microvascular transit time for large vessel.

threshold. If so, the estimated aBV_{LV} would be artificially augmented, and τ_m less shortened than it would be otherwise. (The capillary contribution is not of concern here, because capillary velocities are very low to start with (≤ 0.1 cm/s). Thus, even with possible velocity increases of 100% + that have been found during hypercapnia in rodent studies (Villringer *et al*, 1994; Hutchinson *et al*, 2006), the capillary signal would not be subjected to the artifact even at the lowest velocity-encoding level of 3 cm/s.) The opposite scenario is also theoretically possible in which an artifactually diminished arterial compartment could result if vasodilatation exceeds the CBF increase, leading to decreased blood velocity. As an estimate of the potential error, if the arteriolar fraction of the microvasculature is $\sim$20% (van Zijl *et al*, 1998; Uludag *et al*, 2009) and if the whole microvascular volume is $\sim$2% to 2.5% of a voxel (Uludag *et al*, 2009), then the arteriolar volume is $\sim$0.4% to 0.5% of a voxel. This would be the rough maximum amount of artifactual aBV enlargement, if we were to assume the extreme case of the entire arteriolar contribution being shunted from the microvascular compartment to the arteriolar compartment. The actual amount of artifact is likely to be smaller, given the continuum of arteriolar velocities. A possible way to minimize the velocity-encoding artifact is to find the arterial/arteriolar segment with the least reactivity in terms of velocity changes and perform velocity encoding at that level. Another point to note is that complete dephasing of fast arterial spins in all directions was not possible, because the crusher scheme was restricted to the foot–head direction. Nonetheless, we have seen in this study that modulating the strength of the crusher gradients does not significantly alter the behavior of the estimated vascular parameters during visual stimulation and hypercapnia.

Vascular Reactions During Functional Challenges

The primary aim of this study was to examine potential differences in vascular behavior that contribute

to CBF changes. To this end, two functional challenges that are well known to affect CBF increases were selected, with the difference between them being the mechanisms for eliciting CBF increases. Inhaling an increased concentration of CO_2 leads to an increase in global CBF, primarily owing to the increased presence of H+, which decreases brain tissue pH and also triggers vasodilatation to return the brain to equilibrium (Kuschinsky *et al*, 1972). Conversely, visual stimulation generates neuronal activity in the visual cortex, which results in the occurrence of several possible processes. Neurotransmitters (such as nitric oxide) being released could signal local vasodilatation and hyperemia (Attwell and Iadecola, 2002). Conversely, increased oxidative metabolism (Gjedde *et al*, 2002) and its byproducts of CO_2 and H+ could also lead to an increase in local CBF and may also serve the increased O_2 demand (Buxton and Frank, 1997). The exact mechanisms for hyperemia during neuronal activity are still being debated, but in general, the CBF change in neuronal activity is local, may be attributed to various mechanisms, and probably serves more than one purpose (such as byproduct clearance and delivery of glucose and O_2).

In spite of the different neurochemical origins of cerebrovascular activity induced by these challenges, a standard assumption in functional studies is that the consequence on the vascular system will be mechanically similar. In particular, the BOLD calibration method to calculate changes in $CMRO_2$ based on the deoxyhemoglobin dilution model assumes that the volume–flow relationship in hypercapnia is similar to other functional challenges (Davis *et al*, 1998; Hoge *et al*, 1999). In this study, we found not only similarities but also subtle differences in the behavior of the vascular parameters examined under steady-state conditions of hypercapnia, visual stimulation, and a combination of the two. These experimental conditions consistently elicited reductions in the large arterial vessel transit time ($TT_{am,LV}$), which were proportionate to each level of CBF increase. In addition, there were remarkably similar and significant aBV_{GM}–CBF relationships in all three conditions, as evidenced by power law analyses. The relatively high α-values of 0.55 to 0.69 are consistent with the few studies showing significant arterial blood volume responses that correlated with flow increases in rodents during hypercapnia (Lee *et al*, 2001) and sensory stimulation (Kim *et al*, 2007; Kim and Kim, 2010). These studies also show that most of the total CBV changes during hypercapnia and visual stimulation arise from the arterial component. Therefore, if we assume that the capillary and venous blood volume fractions also respond consistently throughout these conditions, our results suggest that the total volume–flow relationship assumption in BOLD calibration may be valid within the occipital gray matter regions and steady-state conditions.

Nevertheless, dissociations of behavior between the large and small (gray matter) arterial vessel compartments were also found. (The large arterial vessel compartment is from the sites of AIF sampling.) During hypercapnia, volume increase of the large arterial vessels (aBV_{LV}) contributed to CBF increase, also as seen with a significant α-value, whereas further downstream in the smaller arteries within the gray matter, transit time ($TT_{am,GM}$) was reduced. Sensitivity to hypercapnia in both large and small cerebral vessels has been shown (Lu *et al*, 2009), and our findings in large and small arterial vessels are in agreement. In contrast, during visual stimulation, changes in aBV_{LV} and $TT_{am,GM}$ were not significant. Furthermore, the relationship of aBV_{LV}–CBF as assessed by a power law function was insignificant. Similar to the condition of hypercapnia alone, the combined condition of hypercapnia and visual stimulation showed a significant aBV_{LV}–CBF relationship and decreased $TT_{am,GM}$, but not to the same extent as in pure hypercapnia. These moderated outcomes in the combined condition may imply that there are certain vascular mechanisms with potentially competing effects during hypercapnia and visual stimulation. Certainly, our understanding of neurovascular coupling in situations with a combination of physiologic challenges is lacking, despite the implications for experimental design and function in disease. Overall, these findings suggest, also in view of the similarities observed, that there are spatially distinct vascular mechanisms along the arterial tree. Spatially heterogeneous vascular behavior has also been observed in capillaries in rats during hypercapnia (Hutchinson *et al*, 2006). It was found that changes in capillary red blood cell velocities occurred mainly in the larger and medium capillaries, whereas volume changes were observed mainly in the small capillaries. Spatial heterogeneity of the exponent α has been shown for hypercapnia and hypocapnia (Wu *et al*, 2002; Rostrup *et al*, 2005). The dissociations in our results go further to show that spatial dependence of the volume–flow relationship is influenced by the nature of the conditions—areas around sizeable arteries show different volume–flow relationships during neurogenic and nonneurogenic conditions, unlike areas with mainly tissue. To find a region-specific α-value for calculations of $CMRO_2$ (cerebral metabolic rate of oxygen) changes based on the BOLD calibration model, exclusion of the large vessel areas may not be entirely straightforward, given the intricate vascular network and the partial volume effect in voxels with current functional magnetic resonance imaging resolution. Nonetheless, this study has shown that at a voxel resolution of $3.5 \times 3.5 \times 5\,mm^3$, the average α-value for the gray matter arterial blood volume to flow relationship, is not significantly different between hypercapnia and visual stimulation steady states.

Although it has been pointed out that α-values seem to be different in various conditions, such as in hypercapnia (Grubb *et al*, 1974) and other functional challenges (Ito *et al*, 2001; Jones *et al*, 2001), these

α-values may not be directly comparable given that the conditions were not studied together, resulting in possible differences between measurement techniques, experimental paradigm, and subjects. However, the one concurrent study that we are aware of in the literature (Jones *et al*, 2002) found a slightly lower α-value for rat barrel cortex stimulation as compared with hypercapnia, although it has to be noted that they assumed CBV changes from total hemoglobin changes, and the surface cortex that they assessed using laser Doppler flowmetry may show a different relationship compared with the deep visual cortex.

Our comparisons of the relationship of arterial blood volume with flow in various conditions have been based on the assumption that the relationship is best described by a power law (Grubb *et al*, 1974). Although it has been observed that volume–flow relationships may also be linearly fitted (Rostrup *et al*, 2005; Piechnik *et al*, 2008), nonlinearities in the relationships of the more extreme values suggest a power law in line with Hagen–Poiseuille's formulae (Grubb *et al*, 1974; van Zijl *et al*, 1998). For the condition of visual stimulation alone, in which an insignificant α-value was found for the relationship of aBV_{LV} to CBF changes, it must be noted that a significant and positive linear trend could be fitted, in which the slope was 0.21 ± 0.09 with intercept 0.76 ± 0.15 (mean ± s.e.m.). The relatively gentle slope indicates that generally aBV_{LV} changes varied positively with CBF changes during visual stimulation, but relatively large individual variation (Figure 6A) resulted in an overall insignificant aBV_{LV} increase during visual stimulation (Table 1). A linear fit of aBV_{GM} with CBF changes in the same condition was not statistically significant. Linear fits of these volume–flow pairs in the hypercapnia and the combined conditions were also not statistically significant, thus indicating that the power law function was a better description of the volume–flow relationships in these other situations.

It is interesting that in the large arterial vessel compartment, changes in transit time during hypercapnia and visual stimulation seemed to balance the arterial volume changes (Figure 6B). Larger aBV_{LV} increases were significantly correlated with smaller $TT_{am,LV}$ reductions, although intriguingly not in the combined condition. The complementary behavior was not evident in the smaller, gray matter arterial vessels. This again points to the likelihood of spatially distinct vascular mechanisms. On the basis of the central volume principle (flow = volume/mean transit time), the balance of volume with transit time changes could serve to moderate flow in the larger arterial segments. The lack of significant correlations in the smaller arterial (gray matter) compartment reflects the considerable independence of changes in aBV_{GM} with changes in $TT_{am,GM}$; the latter could be caused by upstream or downstream pressure changes. It helps to explain the potential inconsistency that aBV_{GM} and CBF could show remarkably similar relationships during hypercapnia and visual stimulation, even though $TT_{am,GM}$ did not respond significantly during visual stimulation, unlike during hypercapnia.

With hypercapnia, CBF increased on average by ~21%, which is considerably lower than what would be expected given the mean 14 mm Hg increase in end-tidal pCO_2. However, our end-tidal pCO_2 could have been overestimated because of contamination of the expired gas sampling by the inflowing CO_2 gas mixture, as the respiratory mask used allows mixing of the inflowing and expired gases. The lack of response in the respiratory rate during hypercapnia supports this likelihood. Nonetheless, there was sufficient perturbation of the vascular system in the hypercapnic condition that allowed us to observe significant vascular responses.

Although it is tempting to attribute our results wholly to the different physiologic states elicited by the hypercapnic challenge and visual stimulation, we cannot exclude the possibility that the results could also reflect differences in the amplitudes of CBF change. The hypercapnic CBF increase was about a third of the CBF increase that was attributed to visual stimulation. Thus, perhaps when flow increases are low, increases are modulated mainly through aBV_{LV} and $TT_{am,GM}$, whereas $TT_{am,LV}$ and aBV_{GM} are responsible for larger flow increases. Another possible difference that these results could reflect is that the hypercapnic condition lasted longer than the visual stimulation, and thus the vascular responses could have evolved differently over the longer duration of the hypercapnic challenge (Mandeville *et al*, 1999*a*). Nonetheless, in the combined condition of hypercapnia and visual stimulation, which elicited the largest CBF change, we see an averaging of the different vascular effects observed in hypercapnia or visual stimulation alone. Therefore, it is unlikely that the phenomena observed are simply caused by CBF amplitude or duration of experimental manipulation alone. Nevertheless, there could be multiple influences, which could be separated in a further study controlling all these factors.

This study adds to the growing body of evidence for significant changes in arterial blood volume during functional challenges, such as hypercapnia (Lee *et al*, 2001), visual stimulation (Kim *et al*, 2007; Kim and Kim, 2010), and finger-tapping (Brookes *et al*, 2007). Changes in arterial blood volume were earlier assumed to be negligible in the modeling of the BOLD signal (Buxton *et al*, 1998; Mandeville *et al*, 1999*b*), but including a reactive arterial blood volume fraction provides a better fit to the BOLD experimental data (Blockley *et al*, 2009).

In conclusion, this study provides a detailed look at the vascular dynamics in arterial segments concurrent with CBF changes during the separate conditions of hypercapnia and visual stimulation, and also a combination of the two. It is clear that within the neurovascular system, there is much complexity to be appreciated and some of this

appears to be spatially dependent and condition specific. Nonetheless, together with a consistent reduction in transit time from large arterial to microvessels, a consistent arterial volume–flow relationship was found for the gray matter in the visual cortex under our specific conditions. Varying the level of velocity encoding between Venc = 3 cm/s to Venc = 9 cm/s does not appear to significantly alter the estimated CBF, nor does it alter the pattern of significant responses in the two physiologic challenges. This may allow the comparison of ΔCBF results across functional studies that use different levels of vascular crushers within the investigated range.

Acknowledgements

We thank Kristjana Yonsdottir for statistical advice and Albert Gjedde for insightful comments.

Disclosure/conflict of interest

The authors declare no conflict of interest.

References

Attwell D, Iadecola C (2002) The neural basis of functional brain imaging signals. *Trends Neurosci* 25:621–5

Blockley NP, Francis ST, Gowland PA (2009) Perturbation of the BOLD response by a contrast agent and interpretation through a modified balloon model. *Neuroimage* 48:84–93

Britz GW, Meno JR, Park IS, Abel TJ, Chowdhary A, Nguyen TS, Winn HR, Ngai AC (2007) Time-dependent alterations in functional and pharmacological arteriolar reactivity after subarachnoid hemorrhage. *Stroke* 38:1329–35

Brookes MJ, Morris PG, Gowland PA, Francis ST (2007) Noninvasive measurement of arterial cerebral blood volume using Look-Locker EPI and arterial spin labeling. *Magn Reson Med* 58:41–54

Buxton RB, Frank LR (1997) A model for the coupling between cerebral blood flow and oxygen metabolism during neural stimulation. *J Cereb Blood Flow Metab* 17:64–72

Buxton RB, Frank LR, Wong EC, Siewert B, Warach S, Edelman RR (1998) A general kinetic model for quantitative perfusion imaging with arterial spin labeling. *Magn Reson Med* 40:383–96

Davis TL, Kwong KK, Weisskoff RM, Rosen BR (1998) Calibrated functional MRI: mapping the dynamics of oxidative metabolism. *Proc Natl Acad Sci USA* 95:1834–9

Gilmore ED, Hudson C, Preiss D, Fisher J (2005) Retinal arteriolar diameter, blood velocity, and blood flow response to an isocapnic hyperoxic provocation. *Am J Physiol Heart Circ Physiol* 288:H2912–7

Gjedde A, Marrett S, Vafaee M (2002) Oxidative and nonoxidative metabolism of excited neurons and astrocytes. *J Cereb Blood Flow Metab* 22:1–14

Gowland P, Mansfield P (1993) Accurate measurement of T1 *in vivo* in less than 3 seconds using echo-planar imaging. *Magn Reson Med* 30:351–4

Grubb RL, Jr, Raichle ME, Eichling JO, Ter Pogossian MM (1974) The effects of changes in $PaCO_2$ on cerebral blood volume, blood flow, and vascular mean transit time. *Stroke* 5:630–9

Herscovitch P, Raichle ME (1985) What is the correct value for the brain—blood partition coefficient for water? *J Cereb Blood Flow Metab* 5:65–9

Ho YC, Petersen ET, Golay X (2010) Measuring arterial and tissue responses to functional challenges using arterial spin labeling. *Neuroimage* 49:478–87

Hoge RD, Atkinson J, Gill B, Crelier GR, Marrett S, Pike GB (1999) Linear coupling between cerebral blood flow and oxygen consumption in activated human cortex. *Proc Natl Acad Sci USA* 96:9403–8

Hutchinson EB, Stefanovic B, Koretsky AP, Silva AC (2006) Spatial flow-volume dissociation of the cerebral microcirculatory response to mild hypercapnia. *Neuroimage* 32:520–30

Ito H, Kanno I, Ibaraki M, Suhara T, Miura S (2008) Relationship between baseline cerebral blood flow and vascular responses to changes in $PaCO_2$ measured by positron emission tomography in humans: implication of inter-individual variations of cerebral vascular tone. *Acta Physiol (Oxf)* 193:325–30

Ito H, Takahashi K, Hatazawa J, Kim SG, Kanno I (2001) Changes in human regional cerebral blood flow and cerebral blood volume during visual stimulation measured by positron emission tomography. *J Cereb Blood Flow Metab* 21:608–12

Jones M, Berwick J, Johnston D, Mayhew J (2001) Concurrent optical imaging spectroscopy and laser-Doppler flowmetry: the relationship between blood flow, oxygenation, and volume in rodent barrel cortex. *Neuroimage* 13:1002–15

Jones M, Berwick J, Mayhew J (2002) Changes in blood flow, oxygenation, and volume following extended stimulation of rodent barrel cortex. *Neuroimage* 15:474–87

Kety SS, Schmidt CF (1948) The effects of altered arterial tensions of carbon dioxide and oxygen on cerebral blood flow and cerebral oxygen consumption of normal young men. *J Clin Invest* 27:484–92

Kim T, Hendrich KS, Masamoto K, Kim SG (2007) Arterial versus total blood volume changes during neural activity-induced cerebral blood flow change: implication for BOLD fMRI. *J Cereb Blood Flow Metab* 27: 1235–47

Kim T, Kim SG (2010) Cortical layer-dependent arterial blood volume changes: improved spatial specificity relative to BOLD fMRI. *Neuroimage* 49:1340–9

Kisilevsky M, Mardimae A, Slessarev M, Han J, Fisher J, Hudson C (2008) Retinal arteriolar and middle cerebral artery responses to combined hypercarbic/hyperoxic stimuli. *Invest Ophthalmol Vis Sci* 49:5503–9

Kleinfeld D, Mitra PP, Helmchen F, Denk W (1998) Fluctuations and stimulus-induced changes in blood flow observed in individual capillaries in layers 2 through 4 of rat neocortex. *Proc Natl Acad Sci USA* 95:15741–6

Kobari M, Gotoh F, Fukuuchi Y, Tanaka K, Suzuki N, Uematsu D (1984) Blood flow velocity in the pial arteries of cats, with particular reference to the vessel diameter. *J Cereb Blood Flow Metab* 4:110–4

Kuschinsky W, Wahl M, Bosse O, Thurau K (1972) Perivascular potassium and pH as determinants of local

pial arterial diameter in cats. A microapplication study. *Circ Res* 31:240–7

Lee SP, Duong TQ, Yang G, Iadecola C, Kim SG (2001) Relative changes of cerebral arterial and venous blood volumes during increased cerebral blood flow: implications for BOLD fMRI. *Magn Reson Med* 45:791–800

Leontiev O, Buxton RB (2007) Reproducibility of BOLD, perfusion, and CMRO2 measurements with calibrated-BOLD fMRI. *Neuroimage* 35:175–84

Lu J, Dai G, Egi Y, Huang S, Kwon SJ, Lo EH, Kim YR (2009) Characterization of cerebrovascular responses to hyperoxia and hypercapnia using MRI in rat. *Neuroimage* 45:1126–34

Mandeville JB, Marota JJ, Ayata C, Moskowitz MA, Weisskoff RM, Rosen BR (1999*a*) MRI measurement of the temporal evolution of relative CMRO(2) during rat forepaw stimulation. *Magn Reson Med* 42:944–51

Mandeville JB, Marota JJ, Ayata C, Zaharchuk G, Moskowitz MA, Rosen BR, Weisskoff RM (1999*b*) Evidence of a cerebrovascular postarteriole windkessel with delayed compliance. *J Cereb Blood Flow Metab* 19:679–89

Panczel G, Daffertshofer M, Ries S, Spiegel D, Hennerici M (1999) Age and stimulus dependency of visually evoked cerebral blood flow responses. *Stroke* 30:619–23

Petersen ET, Lim T, Golay X (2006) Model-free arterial spin labeling quantification approach for perfusion MRI. *Magn Reson Med* 55:219–32

Piechnik SK, Chiarelli PA, Jezzard P (2008) Modelling vascular reactivity to investigate the basis of the relationship between cerebral blood volume and flow under CO_2 manipulation. *Neuroimage* 39:107–18

Rostrup E, Knudsen GM, Law I, Holm S, Larsson HB, Paulson OB (2005) The relationship between cerebral blood flow and volume in humans. *Neuroimage* 24:1–11

Uludag K, Muller-Bierl B, Ugurbil K (2009) An integrative model for neuronal activity-induced signal changes for gradient and spin echo functional imaging. *Neuroimage* 48:150–65

van Zijl PC, Eleff SM, Ulatowski JA, Oja JM, Ulug AM, Traystman RJ, Kauppinen RA (1998) Quantitative assessment of blood flow, blood volume and blood oxygenation effects in functional magnetic resonance imaging. *Nat Med* 4:159–67

Villringer A, Them A, Lindauer U, Einhaupl K, Dirnagl U (1994) Capillary perfusion of the rat brain cortex. An *in vivo* confocal microscopy study. *Circ Res* 75:55–62

Wong EC, Buxton RB, Frank LR (1998) Quantitative imaging of perfusion using a single subtraction (QUIPSS and QUIPSS II). *Magn Reson Med* 39:702–8

Wu G, Luo F, Li Z, Zhao X, Li SJ (2002) Transient relationships among BOLD, CBV, and CBF changes in rat brain as detected by functional MRI. *Magn Reson Med* 48:987–93

Ye FQ, Mattay VS, Jezzard P, Frank JA, Weinberger DR, McLaughlin AC (1997) Correction for vascular artifacts in cerebral blood flow values measured by using arterial spin tagging techniques. *Magn Reson Med* 37:226–35